nature food

Article

https://doi.org/10.1038/s43016-022-00613-9

Increasing dominance of Indian Ocean variability impacts Australian wheat yields

Received: 20 February 2022

Accepted: 8 September 2022

Published online: 13 October 2022

Check for updates

Puyu Feng[1] ✉, Bin Wang[2] ✉, Ian Macadam[3,4], Andréa S. Taschetto[3,4], Nerilie J. Abram[5,6], Jing-Jia Luo[7], Andrew D. King[8,9], Yong Chen[1], Yi Li[10], De Li Liu[2,11], Qiang Yu[12,13] and Kelin Hu[1] ✉

The relationships between crop productivity and climate variability drivers are often assumed to be stationary over time. However, this may not be true in a warming climate. Here we use a crop model and a machine learning algorithm to demonstrate the changing impacts of climate drivers on wheat productivity in Australia. We find that, from the end of the nineteenth century to the 1980s, wheat productivity was mainly subject to the impacts of the El Niño Southern Oscillation. Since the 1990s, the impacts from the El Niño Southern Oscillation have been decreasing, but those from the Indian Ocean Dipole have been increasing. The warming climate has brought more occurrences of positive Indian Ocean Dipole events, resulting in severe yield reductions in recent decades. Our findings highlight the need to adapt seasonal forecasting to the changing impacts of climate variability to inform the management of climate-induced yield losses.

Rapid increases in global population and affluence call for increased quantity in food supply. Although the impacts of climate warming on agriculture may vary in different regions[1], overall, global agriculture will need to double its production of major cereal crops to feed 10 billion people by the 2050s, translating to a ~2.4% growth in crop production per year (ref. [2]). As food systems are increasingly globalized and interdependent, it is expected that a large portion of this growth will come from an increase in crop yields in the countries that are currently the primary crop-producing and crop-exporting countries. However, maintaining stable crop yields in these countries (especially with a Mediterranean climate) is challenging as year-to-year climate variability often subjects crops to unfavourable climate conditions, including floods, droughts and heat stress.

The climate variability can be managed by optimizing farm inputs (for example, seed and fertilizer) in potentially 'good' or 'bad' seasons if weather anomalies can be reliably informed in advance. However, skilful weather forecasts are reliable only within a 2-week horizon, which is usually not enough for cultivation plans to be made in terms of seasonal crops. Instead, producers are increasingly being informed by seasonal forecasts that rely on the behaviour of large-scale climate drivers. Weather conditions (for example, rainfall and temperature) in many regions can be regularly influenced by large-scale climate drivers from surrounding oceans[3,4], such as the El Niño Southern Oscillation

[1]College of Land Science and Technology, China Agricultural University, Key Laboratory of Arable Land Conservation (North China), Ministry of Agriculture, Beijing, PR China. [2]NSW Department of Primary Industries, Wagga Wagga Agricultural Institute, Wagga Wagga, New South Wales, Australia. [3]ARC Centre of Excellence for Climate Extremes, University of New South Wales, Sydney, New South Wales, Australia. [4]Climate Change Research Centre (CCRC), University of New South Wales, Sydney, New South Wales, Australia. [5]Research School of Earth Sciences, Australian National University, Canberra, Australian Capital Territory, Australia. [6]ARC Centre of Excellence for Climate Extremes, Australian National University, Canberra, Australian Capital Territory, Australia. [7]Institute for Climate and Application Research (ICAR)/CICFEMD/KLME/ILCEC, Nanjing University of Information Science and Technology, Nanjing, PR China. [8]School of Geography, Earth, and Atmospheric Sciences, University of Melbourne, Melbourne, Victoria, Australia. [9]ARC Centre of Excellence for Climate Extremes, University of Melbourne, Melbourne, Victoria, Australia. [10]College of Water Resources and Architectural Engineering, Northwest A&F University, Yangling, PR China. [11]Climate Change Research Centre, University of New South Wales, Sydney, New South Wales, Australia. [12]State Key Laboratory of Soil Erosion and Dryland Farming on the Loess Plateau, Institute of Soil and Water Conservation, Northwest A&F University, Yangling, PR China. [13]Key Laboratory of Water Cycle and Related Land Surface Processes, Institute of Geographic Sciences and Natural Resources Research, Chinese Academy of Sciences, Beijing, PR China. ✉e-mail: fengpuyu@cau.edu.cn; bin.a.wang@dpi.nsw.gov.au; hukel@cau.edu.cn

https://doi.org/10.1038/s43016-022-00613-9

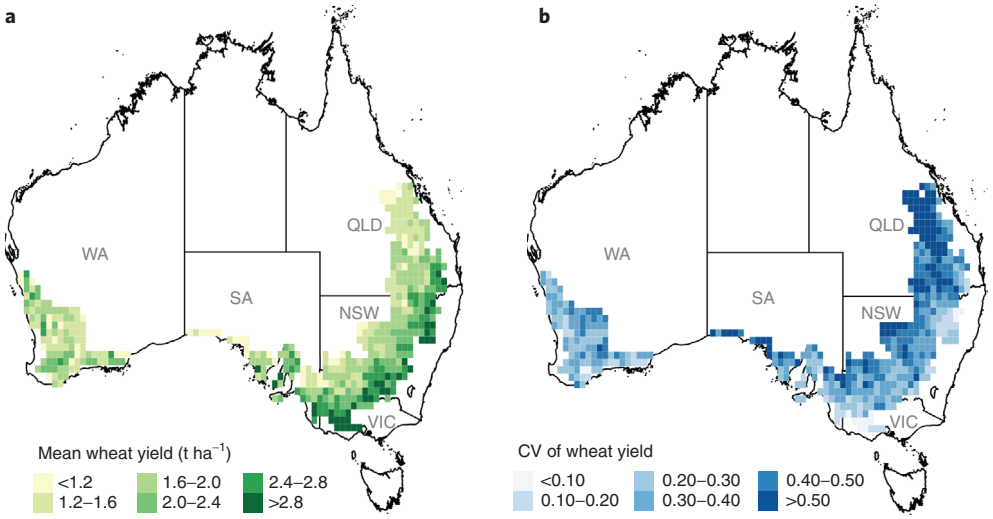

Fig. 1 | Simulated wheat yield across Australian wheatbelt. a,**b**, Mean (**a**) and CV (**b**) of wheat yield during years 1889–2020. WA, Western Australia; SA, South Australia; VIC, Victoria; NSW, New South Wales; QLD, Queensland. Wheat yield was simulated by a well-calibrated biophysical crop model, APSIM (https://www.apsim.info/), for 0.5° grid cells throughout the wheatbelt. The model was driven by the SILO gridded climate dataset, including daily rainfall, solar radiation, and maximum and minimum air temperatures from 1889 to 2020.

(ENSO), the most prominent inter-annual phenomenon in the tropical Pacific. Consequently, there is a relation chain that climate drivers modulate local weather that affect crop productivity. Furthermore, scientific advances have improved the skill in forecasting the dynamics of climate drivers, with lead times ranging from several months up to a year[5]. Farmers can benefit from the routine availability of climate driver forecasts by changing their strategies to adapt to the upcoming season.

The relationships between crop productivity and climate drivers are generally region specific. However, ENSO has been shown to be a dominant driver, with over 28% of global cropland subjected to considerable impacts of ENSO anomalies during 1961–2010 (ref. [6]). ENSO-based seasonal climate or crop yield forecasting approaches for different regions were developed decades ago[7,8]. These are mostly derived from traditional linear regression or correlation analyses that do not allow for potential non-linear changes in the impacts of ENSO or changes in the relative importance of different climate drivers that could develop under a background of climate warming. Previous studies have revealed that climate drivers are non-stationary phenomena, and their characteristics (for example, spatial patterns, variance, duration and frequency) and impacts on regional climate conditions can change over time. For example, ENSO characteristics can change over time[9], and its impacts can be modified by modes of climate variability operating on inter-decadal and longer timescales[10].

Australia is one of the world's largest producers and exporters of wheat, accounting for 10–15% of annual global wheat exports. Consequently, Australia plays a key role in global food supply at present, and is expected to continue to do so in the future. It is well established that inter-annual variability of Australia's climate is heavily influenced by climate drivers from the three surrounding oceans: ENSO in the Pacific Ocean, the Indian Ocean Dipole (IOD, an east–west gradient of sea surface temperature (SST) across the tropical Indian Ocean), and the Southern Annular Mode (SAM, a north–south movement of the mid-latitude circumpolar westerly winds) over the Southern Ocean[3,11,12]. IOD variability is being altered by climate change[13] and has played a more important role in several severe drought events in Indian-Ocean-rim countries during recent decades[14,15]. Similarly, climate change is resulting in changes in SAM that are outside the range of pre-industrial natural variability of the last millennium[16]. Therefore, it is likely that the impacts of large-scale climate drivers on crop yields are not stable. In this Article, we use the Australian wheatbelt as a case region to explore the potential changing impacts of climate drivers on crop yields. Improving our understanding of any changes in the impacts of these climate drivers on Australian wheat productivity has important implications for increasing the resilience of global food production.

Results

Descriptive statistics of wheat productivity and climate drivers

Climate drivers can change from decade to decade. To sample this variation, long-term datasets of climate drivers and crop yields are needed to evaluate potential changes in climate variability and its impacts on crop yields. Long-term climate driver data are relatively easy to obtain, but observed crop yield datasets at century scale are rare. An additional challenge is that it is difficult to isolate the impacts of climate fluctuations on crop productivity in such datasets, as change in observed crop yields is also driven by many other non-climatic factors, including changes in agronomic management practices and technology development. We address these challenges by simulating wheat yield data with rainfall, solar radiation, and maximum and minimum temperature from a climate dataset starting in 1889, with all other non-climatic factors kept constant through time. Figure 1 presents the mean and coefficient of variation (CV) of simulated annual wheat yields during 1889–2020 for 0.5° grid cells across the Australia wheatbelt. The average simulated wheat yield of the wheatbelt is around 2.0 t ha^{-1}, with yields in the eastern and south-eastern fringe of the belt being higher than in other areas. The mean CV of wheat yield across the Australian wheatbelt is 0.38. Australian wheat is generally grown under rainfed conditions and is highly sensitive to rainfall variability (Supplementary Fig. 1). Hence, low yields and larger-than-average variation are found in more inland areas, on the fringe of the arid interior of the Australian continent.

We use the Southern Oscillation Index (SOI)[17], the Dipole Mode Index (DMI)[18] and the SAM index[19] to characterize the occurrence and magnitude of ENSO, IOD and SAM phases, respectively. The SOI measures the difference in sea level pressure (SLP) between the western and central tropical Pacific. Sustained negative (positive) SOI values indicate El Niño (La Niña) events, typically bringing lower (higher) than average winter–spring rainfall across eastern and northern regions of Australia. The DMI is defined as the difference between the SST anomalies of western and eastern regions of the equatorial Indian Ocean. A positive IOD event (sustained positive DMI values) typically results

https://doi.org/10.1038/s43016-022-00613-9

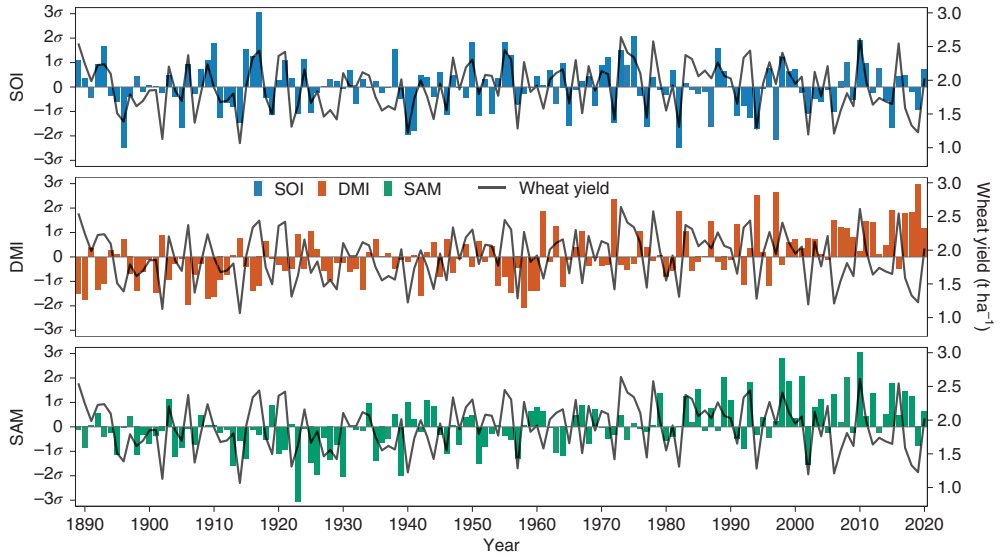

Fig. 2 | Annual mean Australian national wheat yield (black lines) and growing season mean climate driver indices (bars) during 1889–2020. The left *y* axis represents the normalized values of three climate driver indices, the SOI, the DMI and the SAM index. The right *y* axis represents simulated wheat yields.

in below-average winter–spring rainfall over western and southern Australia, but above-average winter–spring rainfall during a negative event. The SAM index is the difference in zonal mean SLP between 40° S and 65° S. The effects of the SAM on Australia's winter rainfall vary greatly depending on region (that is, more (less) rainfall in the east and less (more) rainfall in the south during a positive (negative) phase). Australian wheat is generally grown from late autumn to late spring. It is therefore anticipated that there are associations between climate drivers and wheat yields.

Figure 2 shows the temporal variations of wheat yield as well as growing season (May to November) mean climate driver indices during 1889–2020. Wheat yield varied greatly over the study period, ranging from 1.1 t ha^{-1} in 1914 to 2.6 t ha^{-1} in 1973. The responses of yield to climate drivers are generally consistent with previous results suggesting that positive-phase IOD and El Niño events negatively impact Australian national wheat yield[20]. For example, national wheat yield was low in 1914, 1940, 1982 and 2019, years experiencing a positive IOD or El Niño phase. As for SAM, it does not show a consistent effect on national yield. While there are no apparent long-term trends in the SOI over the study period, there is a clear long-term signal in both DMI and SAM, with many positive-phase years in recent decades but seldom during the first half of the study period. It should be noted that nearly every positive IOD phase year witnesses a yield reduction, even with neutral phases of ENSO (for example, 2019). It is likely that a shift in the relative contributions of climate drivers to yield variations may occur.

Changes of dominant climate drivers

We identify the dominant climate driver for each grid over different time periods across the wheatbelt, and the stationarity of the local-scale impacts of these climate drivers over time. We equally split the 1889–2020 dataset into four 33 year subperiods, namely 1889–1921, 1922–1954, 1955–1987 and 1988–2020. Our hypothesis is that the impacts of the different drivers on crop productivity differ between subperiods. We restrict our analysis to four 33 year subperiods as this is near to the accepted 30 year convention to define climatology and maintains enough samples of different phases of climate drivers in each period for subsequent analysis. Given that IOD can co-occur with ENSO (Supplementary Table 1), we remove the influence of ENSO from IOD using a simple linear regression[21].

The dominant climate driver has varied over time in most grids. During the first subperiod (1889–1921), ENSO was the dominant climate driver in most grids of the wheatbelt (Fig. 3a). The IOD and the SAM were only dominant in sporadic grids throughout the wheatbelt. During the second subperiod (1922–1954), the importance of the SAM increased, exhibiting greater impacts on wheat yield in many southern grids (Fig. 3b). Eastern and north-eastern areas continued to be dominated by ENSO. In the following subperiod (1955–1987), ENSO presented enhanced effects on wheat yield and recaptured many grids that were previously dominated by SAM (Fig. 3c). During the most recent subperiod (1988–2020), the dominant climate drivers over the wheatbelt shifted greatly (Fig. 3d). The IOD became the dominant driver across southern parts of the wheatbelt. Only north-eastern areas and some grids in the west were dominated by ENSO or SAM. This phenomenon is rarely seen in the past century (Supplementary Fig. 2).

Shifting impacts of climate drivers on wheat productivity

The results for the first three subperiods (Fig. 3) show that, between 1889 and 1987, ENSO was consistently the most widespread influence on variability in wheat yield, particularly in eastern regions. However, since 1988, influences from the Indian Ocean far exceeded those from the Pacific. This is consistent with Yuan and Yamagata's study[20], who demonstrated stronger negative impacts of IOD than ENSO on wheat yields in recent decades. Severe drought and bushfire events during the recent three decades have also been attributed to more occurrences of positive IOD rather than ENSO[15,22,23]. Interestingly, the mean and CV of simulated wheat yield have been relatively stable from one climatological period to the next (though not on shorter timescales), despite the great changes of dominant climate drivers (Supplementary Fig. 3). It is likely that the magnitude of variability in wheat yields due to the influence of different climate drivers is similar in different subperiods, but their relative contributions change. The changing dominance of the climate drivers may be due to changes in the relationships between the drivers and yields.

Non-linear relationships are detected between wheat yields and climate drivers (Fig. 4). In general, the effects of the climate drivers on wheat yields are non-stationary. The effects of ENSO on wheat yields were slightly stronger during 1889–1921 and 1955–1987, as denoted by larger average slopes. In these two subperiods, more grids were also identified to be dominated by ENSO (Supplementary Fig. 4). The sensitivity of yields to the IOD was also non-stationary over time, being greater during 1988–2020 than in the earlier periods. This, plus a high degree of variability in the IOD (that is, more occurrences of positive

https://doi.org/10.1038/s43016-022-00613-9

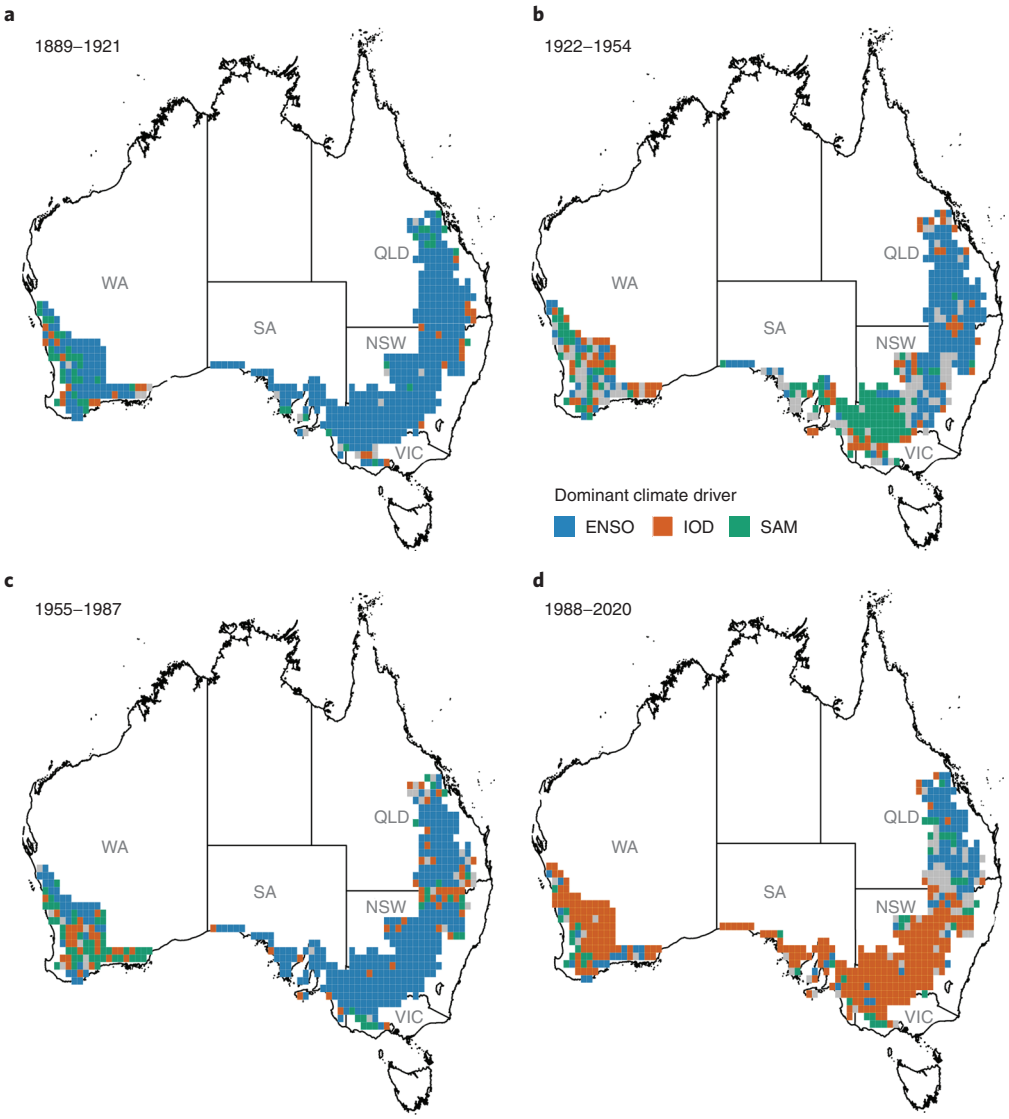

Fig. 3 | Dominant climate driver of wheat yield at each grid as identified by the RF model. a–d, Dominant climate driver of wheat yield for the years 1889–1921 (**a**), 1922–1954 (**b**), 1955–1987 (**c**) and 1988–2020 (**d**). The grey grids indicate where no single driver is dominant. Dominance is determined when an importance value is more than 50% for a specific driver based on the RF model.

IOD events; Fig. 2), explains why the IOD was identified as the dominant climate driver across most of the wheatbelt in the fourth subperiod. The effect of SAM was also enhanced in the fourth subperiod, but it was still relatively weaker than that of IOD. In addition, the curves in Fig. 4 also suggest the asymmetric impacts of positive and negative events of climate drivers. Specifically, the impact of a positive event on wheat yield is not necessarily the precise opposite of the impact of a negative event. This is mainly because the relationships between climate drivers and Australia's rainfall are non-linear[24,25].

Contributions of oceanic warming to the shift

An increase was observed in both the mean and the magnitude of variability in DMI (Supplementary Fig. 5), resulting in more occurrences of positive IOD events during the recent subperiod. We note that the Indian Ocean has been warming since 1950 at a higher rate than the other tropical basins[26], and a component of this warming resembles the SST pattern associated with the positive phase of the IOD[27]. A question arises here: is the increasing influence of IOD on yields related to this long-term warming trend? Next, we study the effects of oceanic warming on the shifting influence of IOD by re-running the random forest (RF) model with detrended DMI series. Spatial distributions of dominant climate drivers in the first three subperiods changed slightly, but changed greatly in the fourth subperiod, with more grids dominated by ENSO or SAM rather than IOD (Supplementary Fig. 6). This suggests that the increasing influence of IOD is partly related to the multi-decadal warming trend in the Indian Ocean. This is supported by an analysis of the importance values of the three climate drivers before and after detrending DMI for the fourth subperiod (Fig. 5). The relative contribution of IOD to the yield variability decreases by 18.1% on average after detrending. The importance values of ENSO and SAM increased by 6.2% and 6.9%, respectively.

Discussion

Reliable forecasts of climate drivers are available seasons ahead. Recent scientific advances have demonstrated that decision-makers can make use of this high predictability to improve food monitoring or famine early warning systems, based on the historical relationships between climate drivers and crop yields[6]. Here we show that the relationships are not stationary and can change notably over time. In particular, wheat yield in Australia was mainly subjected to ENSO from the Pacific.

https://doi.org/10.1038/s43016-022-00613-9

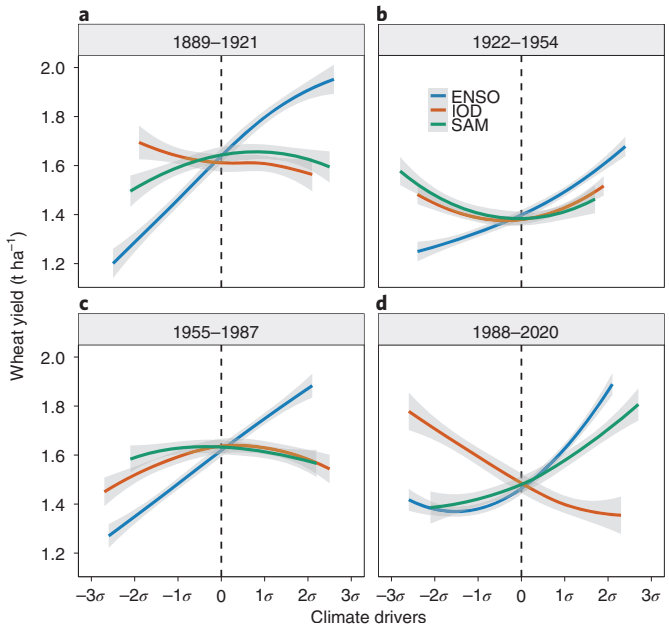

Fig. 4 | Partial dependence of wheat yield change on large-scale climate drivers in four subperiods as derived from the RF model. a–d, Partial dependence of wheat yield change on large-scale climate drivers for the years 1889–1921 (**a**), 1922–1954 (**b**), 1955–1987 (**c**) and 1988–2020 (**d**). Values of climate driver indices are shown as growing season mean values and are normalized. The lines in each panel are smoothed representations of the responses, with averaged fitted values (model predictions based on the data) for 0.5° grid cells over the Australian wheatbelt. The trend of the line, rather than the actual values, describes the nature of the dependence between response and predictor variables. The grey shading shows 95% confidence intervals.

However, since the 1990s, the impacts from ENSO have been decreasing, but those from the IOD have been increasing. The shifting impacts of climate drivers on wheat productivity are through their modulation of Australia's rainfall (Supplementary Fig. 7).

The impacts of the climate drivers on Australia are often compounded and can interact with one another. For example, positive IOD events often occur during El Niño years (Fig. 2), promoting hotter and drier conditions in southeast Australia. In our study, growing season mean SOI and DMI indeed show a significant correlation (Supplementary Table 1). However, after removing the potential dependency of DMI on SOI, the IOD's impacts still become stronger across most of the wheatbelt (Fig. 3). How do the shifting impacts occur? It is well known that the relationship between ENSO and Australian rainfall is modulated on multi-decadal timescales by the Interdecadal Pacific Oscillation[10], a low-frequency pattern of SST variability in the tropical and extra-tropical Pacific. Stronger rainfall response to ENSO events is observed during the negative phase of the IPO. This may be one of the reasons for the increasing dominance of SAM during 1922–1954 (Fig. 3b), when a positive IPO phase probably reduced the influence of ENSO on Australian rainfall. However, since 1999, the IPO has been in a negative phase. Thus, the increasing dominance of IOD may not be related to the weakening of ENSO–Australian rainfall relationship. However, we find that the non-uniform warming of the Indian Ocean contributes to the importance of IOD in recent decades by 18.1%. Multiple lines of evidence imply that the recent trend towards more frequent positive IOD events is related to global warming, and positive IOD events may occur more often over the twenty-first century if greenhouse gas concentrations continue to increase[13,28].

Our study is an important step towards understanding the shifting impacts of climate drivers on crop productivity, which can inform improved climate resilience of regional crop production in the face of climate hazards. For example, drought is a major hazard to Australian wheat production, and prolonged drought in recent years has broken the long-term increasing trend in Australian wheat yields. Many farmers in Australia still rely on the forecasts of the ENSO to prepare for potential drought risk months in advance. An SOI-based seasonal rainfall forecasting programme is officially operated by the Queensland government[8]. However, the impacts from the Indian and Southern Oceans receive less attention. Here we show that, across most of the Australian wheatbelt, the impacts of the IOD have been increasing in recent decades. More occurrences of positive IOD events in the future are also likely to induce more drought events. Thus, we appeal to farmers to consider dynamical model-based seasonal prediction systems when planning their crop management strategies for the upcoming season, such as the Australian Community Climate Earth System Simulator-Seasonal version 1 (ACCESS-S1) developed by the Bureau of Meteorology[29]. Compared with traditional statistically based systems, ACCESS-S1 implicitly accounts for all the modes of climate variability. Nonetheless, there still remain issues with lack of skill beyond a few weeks lead time and occasional forecast busts. This highlights the value of research to improve the simulation of Indian Ocean conditions, and the complex atmospheric links between oceans and the Australian climate, by seasonal forecasting models. These models should ideally produce forecasts whose reliability is robust to changes in the relative importance of different climate drivers due to global warming and low-frequency modes of variability, such as the IPO.

The results of our study can also improve the ability of crop simulation models to generate optimized farming practices for the upcoming season. For example, the SOI phases for the season ahead have been incorporated into the Agricultural Production Systems sIMulator (APSIM) crop model (we used in our study), to explore broad and specific options to adapt wheat cropping systems to ENSO in Australia[30]. Genotypes, sowing dates and nitrogen applications can be tested through scenario simulations at the site level before sowing, when local wheat producers make their most crucial management decisions. Given that our results show that the role of IOD in determining Australian wheat yields becomes more prominent, we also recommend incorporating the IOD into the APSIM model, to improve the agronomic decision-making capabilities.

Finally, our study proposes a method to identify the shift of dominant climate drivers in a world major wheat production area, Australia. However, we believe it can be easily extended to other areas more reliant on subsistence farming of crops, for example, in East Africa. With further understanding of the relationships between climate drivers and crop yields in more areas, we can improve our capacity to recognize and manage structured climate risks, thereby enhancing global food security.

Methods

Wheat yield simulations

In this study, we used the well-calibrated biophysical crop model APSIM, a comprehensive model developed in Australia to simulate biological processes in agricultural systems[31]. APSIM has been used in numerous studies of the responses of Australian wheat cropping to climate variations[32,33]. It is able to simulate crop yields accounting for the interactive effects of climate, crop genotype, soil and crop management. Here APSIM simulations were carried out only with changing climate and atmospheric CO_2 concentrations through time; thus, we can infer that these were the only factors that contribute to the simulated variations of wheat yields.

Here we ran APSIM model at 0.5° grid cells across the Australian wheatbelt from 1889 to 2020. Daily climate data for each grid, including rainfall, solar radiation and maximum and minimum air temperature data, were obtained from Scientific Information for Land Owners (SILO) gridded climate dataset[34]. SILO is a database of Australian climate data from 1889 (current to yesterday). SILO's gridded datasets are

https://doi.org/10.1038/s43016-022-00613-9

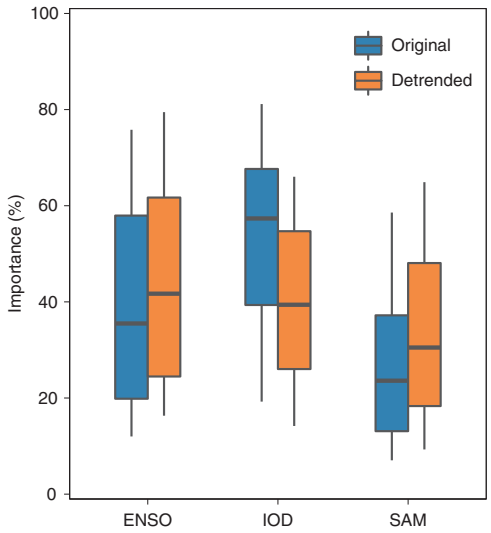

Fig. 5 | Relative importance of large-scale climate drivers on wheat productivity during 1988–2020 before and after detrending the DMI series, derived from the RF model. The black line, two box boundaries and whiskers below and above a box represent median, 25th and 75th percentiles, and 10th and 90th percentiles, respectively.

constructed by spatially interpolating all available observational data. We acknowledge that the changing observational network has implications for the quality of SILO's datasets. Nonetheless, the nature of our analysis and the previous evaluation of gridded datasets alongside their widespread use in previous climate analyses gives us confidence that they may be used for our purposes. First, there were already more than 2,000 rainfall gauge stations in 1890s (https://www.longpaddock.qld.gov.au/silo/about/climate-stations/), and the number has been constantly increasing. Second, spatial and temporal accuracies for gridded datasets are high as described in Jeffrey et al.[34]. For example, average coefficient of determination (R^2) between observed daily variables and interpolated estimates is normally larger than 0.6, especially across the wheatbelt. In addition, SILO datasets are readily available for climate applications and have been well tested in many climate-related studies[35,36].

Soil information for 264 sites (Supplementary Fig. 8) was derived from the APSoil database[31]. Soil attributes of layer depth, bulk density, saturated water content, drained upper limit and crop-specified lower limit were available for each site. For APSIM simulations in a certain grid, soil input information was acquired from the soil site that was geographically closest to the grid. Sowing windows and cultivars were set up according to Wang et al.[37] (Supplementary Table 2) to reflect common farming practices in the different States of Australia. The selected cultivar was sown during the sowing window as soon as the accumulated rainfall exceeds 25 mm in 7 consecutive days, or at the end of sowing window if this condition was not met. The fertilizer at sowing was 130 kg ha^{-1} of urea (equivalent to 60 kg ha^{-1} of N). In addition, the effects of elevated atmospheric CO_2 concentration were also incorporated in accordance with the practice by Wang et al.[37].

We compared APSIM-simulated yields with observed yields to assess the suitability of the simulations for this study. Observed region-level wheat yield records for 2000–2014 in 124 regions were obtained from the yield gap map (http://yieldgapaustralia.com.au/maps/) hosted by the Commonwealth Scientific and Industrial Research Organisation and Grains Research & Development Corporation. As the annual yield series of this dataset was relatively recent, we assumed that variations in yield are caused only by climate variability, and that the contribution of farming technology and practices is negligible. APSIM-simulated yields at grid level were firstly aggregated to region level and then compared with observed yields. The normalized root mean square error (NRMSE) between the simulated and observed yields (15 years × 124 regions) was 14.9% (Supplementary Fig. 9), suggesting that APSIM simulations could potentially capture climate-driven wheat yield variations across the Australian wheatbelt.

$$\mathrm{NRMSE} = \frac{\sqrt{\frac{1}{n}\sum_{i=1}^{n}(S_i - O_i)^2}}{O_{\max} - O_{\min}} \quad (1)$$

where n is the number of samples, S_i and O_i are simulated and observed yields, respectively, and $O_{\max}$ and $O_{\min}$ are maximum and minimum observed yields, respectively. NRMSE represents the relative standard deviation of the residuals. For crop model simulations, performance of a model is considered good if NRMSE is lower than 20%.

Large-scale climate drivers

We used three indices, namely SOI, DMI and SAM index, to characterize the variability of ENSO, IOD and SAM, respectively. There are multiple indices to measure the strength of ENSO events (El Niño, neutral or La Niña). The results of our study varied slightly under different ENSO indices, such as SOI or Niño 3.4 (the average of SST anomalies over the region 5° N–5° S and 170 °W–120° W). We selected SOI because it is based on SLP, a variable more directly linked with rainfall variations than SST. An SST-based ENSO index like Niño 3.4 also incorporates a background warming signal in addition to the natural variability of SSTs, so it has a global warming component as well as an ENSO component, which adds another degree of complexity to examine ENSO. In addition, SOI is also well recognized in Australia, for the estimation of ENSO's impacts. An SOI-based seasonal rainfall forecasting programme is officially operated by the Queensland government[8]. The SOI is calculated as the standardized SLP difference between Tahiti and Darwin, Australia[17]:

$$\mathrm{SOI} = \frac{(\text{standardized Tahiti} - \text{standardized Darwin})}{\mathrm{MSD}} \quad (2)$$

where

$$\text{standardized Tahiti} = \frac{\text{actual Tahiti SLP} - \text{mean Tahiti SLP}}{\text{standard deviation Tahiti}} \quad (3)$$

$$\text{standard deviation Tahiti} = \sqrt{\frac{\sum(\text{actual Tahiti SLP} - \text{mean Tahiti SLP})^2}{N}} \quad (4)$$

$$\text{standardized Darwin} = \frac{\text{actual Darwin SLP} - \text{mean Darwin SLP}}{\text{standard deviation Darwin}} \quad (5)$$

$$\text{standard deviation Darwin} = \sqrt{\frac{\sum(\text{actual Tahiti SLP} - \text{mean Tahiti SLP})^2}{N}} \quad (6)$$

$$\text{MSD (monthly standard deviation)} = \sqrt{\frac{\sum(\text{standardized Tahiti} - \text{standardized Darwin})^2}{N}} \quad (7)$$

and N is the number of months. The anomalies are departures from the 1981–2010 base period.

The DMI is expressed as anomalous SST gradient between the western tropical Indian Ocean (WTIO, 50 °E–70° E and 10 °S–10° N) and the south-eastern tropical Indian Ocean (SETIO, 90° E–110° E and 10° S–0° N) (ref. [18]),

$$\mathrm{DMI} = \text{WTIO SST anomaly} - \text{SETIO SST anomaly} \quad (8)$$

The anomalies are departures from the 1981–2010 base period.

The SAM refers to the (non-seasonal) north–south movement of the strong westerly winds that blow almost continuously in the mid- to high latitudes of the Southern Hemisphere[19]. It is expressed as the difference of zonal mean SLP between 40° S and 65° S,

$$\mathrm{SAM} = \text{standardized } 40°\mathrm{S\ SLP} - \text{standardized } 65°\mathrm{S\ SLP} \quad (9)$$

where each month's zonal mean SLP is standardized by the mean/standard deviation determined for the climatological period (1981–2010). Monthly series of three indices (1889–2020) were obtained from the National Oceanic and Atmospheric Administration Earth System Research Laboratories Physical Sciences Laboratory (https://psl.noaa.gov/). The SOI is calculated on the basis of the observed SLP data from gauge stations. However, no observed SST or SLP from 1889 is available from stations to calculate the DMI or SAM; thus, they are derived from gridded datasets, namely the HadISST1.1 SST dataset and the ICOADS SLP dataset. Although both datasets have been well tested in many climate-related studies[38–40], we acknowledge that their reliability can be slightly different compared with observations, especially in early periods. There were fewer observations available to develop the re-analysis datasets in pre-1900 periods[41]. Growing season (May to November) mean climate drivers were then derived and used as predictor variables in subsequent analysis.

Removal of potential dependency between climate drivers

We noticed a significant negative relationship (Supplementary Table 1) between growing season mean SOI and DMI. To isolate the impact of each climate driver, we removed potential dependency of one index on another using a simple linear regression[21]. Details as following:

$$\widehat{\mathrm{DMI}} = a \times \mathrm{SOI} + b \quad (10)$$

$$\mathrm{DMI\_new} = \mathrm{DMI} - \widehat{\mathrm{DMI}} \quad (11)$$

where $\widehat{\mathrm{DMI}}$ represents predicted DMI values from a linear regression based on SOI. a and b are regression coefficients. DMI_new denotes regression residual, which is linearly independent of SOI and is used in machine learning analysis.

The determination of dominant climate drivers

We implemented a machine learning decision tree model, RF, to study the contributions of growing season climate drivers to wheat yield. RF is a popular tree-based ensemble machine learning algorithm and can be used to investigate the complicated relationships between variables. In contrast to traditional linear regression or correlation analyses, RF accounts for non-linear and hierarchical relationships between the response and predictors. RF builds statistical models using predictor variables and evaluates the relative importance of each predictor variable. In this study, we adopted the accuracy-based importance metric generated from an out-of-bag (OOB) validation procedure. In the model building phase, approximately one-third of the total observational values were randomly selected and set aside for subsequent OOB model validation. Then, the prediction accuracy on the OOB sample was measured. The mean decrease in prediction accuracy when the values of a variable in the OOB sample were randomly shuffled was defined as the importance value of the variable[42], expressed as the mean square error:

$$\mathrm{MSE}_{\mathrm{OOB}} = \frac{1}{n}\sum_{k=1}^{n}\left(O_i - \bar{P}_{\mathrm{kOOB}}\right)^2 \quad (12)$$

where n denotes the number of observations, O_i indicates observed value and $\bar{P}_{\mathrm{kOOB}}$ represents the average of all OOB predictions across all trees. We applied the RF model and derived the importance rankings using the 'caret' package[43] sourced in the R software. We built an RF model for each grid and each subperiod and derived the importance values of predictor variables. The importance values were then normalized to sum to 100%. The predictor variable with an importance value larger than 50% (meaning larger than the sum of the other two drivers) was identified as the dominant climate driver.

According to our results (Fig. 3), the influence of the IOD on wheat yields showed a sudden increase in the final period (1988–2020). To test whether this was random sample error, we calculated the probability that the IOD was the dominant climate driver in any 33 year period before the final period. Specially, we drew a 33 year period from the record (1889–1987) and identified the dominant climate driver with the RF model. We performed this procedure 67 times (year series including 1889–1921, 1890–1922, 1891–1923, …, 1955–1987) at each grid and then calculated the probability that the IOD was the dominant climate driver in all 33 year periods. The results (Supplementary Fig. 2) illustrated that only a small number of grids showed a probability of >0.1, mainly in the west. Most were under 0.1, meaning that a strong influence of the IOD on wheat yields was not usual in 1889–1987.

Partial dependence

We used partial dependence plots (PDPs) to evaluate the marginal effects of predictors (for example SOI, DMI and SAM) on the response variable (wheat yield). A PDP can show whether the relationship between the response and a predictor is linear, monotonic or more complex, marginalizing over the values of all other input predictor variables (the 'complement' features)[44]. Here we used the 'pdp' R package[45] to evaluate the marginal effects of three climate drivers on wheat yield.

The detrending method

There is an increasing trend observed in DMI (Supplementary Fig. 5). We compared the results from the RF models with original DMI and with detrended DMI, to study the potential effects of the trend on the shifting influence of IOD. The method used to detrend the DMI series was the first-difference method introduced by Nicholls[46]. This method was implemented according to the following equation:

$$\Delta\mathrm{DMI}_t = \mathrm{DMI}_t - \mathrm{DMI}_{t-1},\ t = 1890, 1891, \ldots, 2020 \quad (13)$$

where $\Delta\mathrm{DMI}_t$ represents the first difference of DMI at year t, and DMI_t and $\mathrm{DMI}_{t\text{-}1}$ represent the values of DMI at year t and year t–1, respectively. Comparisons of original and detrended values of DMI can be found in Supplementary Fig. 5.

We also compared the performance of the RF models with the original DMI series and with detrended DMI series. We derived NRMSEs from the models with a five-fold cross-validation procedure. This procedure split an input dataset into five non-overlapping groups. In turn, each group was used as a held-back test set, while all other groups collectively were used as a training dataset. A total of five models were fitted and evaluated on the five hold-out test sets and five NRMSEs were reported. Then, the performance of two kinds of models was compared on the basis of their NRMSEs with Fisher's least significant difference method at 95% confidence level. The results (Supplementary Fig. 10) showed that the performance of two kinds of model was similar in most grids, with only a small number of grids presenting significant difference. Thus, in general, detrending the DMI did not affect the performance of the model. Nonetheless, the relative contributions of climate drivers to model performance changed before and after detrending. This is common in an RF model, as the contribution of an input predictor is not fixed, but can change if other input predictors are changed[47].

Reporting summary

Further information on research design is available in the Nature Research Reporting Summary linked to this article.

Data availability

The climate, soil and climate drivers indices data are publicly available from the following sources: the SILO climate data are at https://www.longpaddock.qld.gov.au/silo, the soil data are at https://www.apsim.info/apsim-model/apsoil/ and the climate drivers indices data are at https://psl.noaa.gov/. The detailed wheat yield data simulated by the APSIM crop model and the raw data of the figures are available at Puyu Feng's Github homepage https://github.com/PuyuFeng/NF_Paper.git. Source data are provided with this paper.

Code availability

The detailed R code for data processing and illustration is available at Puyu Feng's Github homepage https://github.com/PuyuFeng/NF_Paper.git.

References

1. Osborne, T., Rose, G. & Wheeler, T. Variation in the global-scale impacts of climate change on crop productivity due to climate model uncertainty and adaptation. *Agric. For. Meteorol.* **170**, 183–194 (2013).
2. Ray, D. K., Mueller, N. D., West, P. C. & Foley, J. A. Yield trends are insufficient to double global crop production by 2050. *PLoS ONE* **8**, e66428 (2013).
3. Ashok, K., Guan, Z. & Yamagata, T. Influence of the Indian Ocean Dipole on the Australian winter rainfall. *Geophys. Res. Lett.* **30**, 1821 (2003).
4. Cai, W., van Rensch, P., Cowan, T. & Hendon, H. H. Teleconnection pathways of ENSO and the IOD and the mechanisms for impacts on Australian rainfall. *J. Clim.* **24**, 3910–3923 (2011).
5. Ludescher, J. et al. Very early warning of next El Niño. *Proc. Natl Acad. Sci. USA* **111**, 2064–2066 (2014).
6. Heino, M. et al. Two-thirds of global cropland area impacted by climate oscillations. *Nat. Commun.* **9**, 1–10 (2018).
7. Phillips, J. G., Cane, M. A. & Rosenzweig, C. ENSO, seasonal rainfall patterns and simulated maize yield variability in Zimbabwe. *Agric. For. Meteorol.* **90**, 39–50 (1998).
8. Stone, R. C., Hammer, G. L. & Marcussen, T. Prediction of global rainfall probabilities using phases of the Southern Oscillation Index. *Nature* **384**, 252–255 (1996).
9. Freund, M. B. et al. Higher frequency of Central Pacific El Niño events in recent decades relative to past centuries. *Nat. Geosci.* **12**, 450–455 (2019).
10. Power, S., Casey, T., Folland, C., Colman, A. & Mehta, V. Inter-decadal modulation of the impact of ENSO on Australia. *Clim. Dyn.* **15**, 319–324 (1999).
11. King, A. D. et al. Extreme rainfall variability in Australia: patterns, drivers, and predictability. *J. Clim.* **27**, 6035–6050 (2014).
12. Risbey, J. S., Pook, M. J., McIntosh, P. C., Wheeler, M. C. & Hendon, H. H. On the remote drivers of rainfall variability in Australia. *Mon. Weather Rev.* **137**, 3233–3253 (2009).
13. Abram, N. J. et al. Palaeoclimate perspectives on the Indian Ocean Dipole. *Quat. Sci. Rev.* **237**, 106302 (2020).
14. King, A. D., Pitman, A. J., Henley, B. J., Ukkola, A. M. & Brown, J. R. The role of climate variability in Australian drought. *Nat. Clim. Chang.* **10**, 177–179 (2020).
15. Ummenhofer, C. C. et al. What causes southeast Australia's worst droughts? *Geophys. Res. Lett.* **36**, L04706 (2009).
16. Abram, N. J. et al. Evolution of the Southern Annular Mode during the past millennium. *Nat. Clim. Chang.* **4**, 564–569 (2014).
17. Ropelewski, C. F. & Jones, P. D. An extension of the Tahiti–Darwin Southern Oscillation Index. *Mon. Weather Rev.* **115**, 2161–2165 (1987).
18. Saji, N. H., Goswami, B. N., Vinayachandran, P. N. & Yamagata, T. A dipole mode in the tropical Indian Ocean. *Nature* **401**, 360–363 (1999).
19. Marshall, G. J. Trends in the Southern Annular Mode from observations and reanalyses. *J. Clim.* **16**, 4134–4143 (2003).
20. Yuan, C. & Yamagata, T. Impacts of IOD, ENSO and ENSO Modoki on the Australian winter wheat yields in recent decades. *Sci Rep.* **5**, 1–8 (2015).
21. Saji, N. H. & Yamagata, T. J. C. R. Possible impacts of Indian Ocean Dipole mode events on global climate. *Clim. Res.* **25**, 151–169 (2003).
22. Cai, W. et al. Opposite response of strong and moderate positive Indian Ocean Dipole to global warming. *Nat. Clim. Chang.* **11**, 27–32 (2021).
23. Wang, B. et al. Extreme fire weather is the major driver of severe bushfires in southeast Australia. *Sci. Bull.* **67**, 655–664 (2022).
24. Cai, W., van Rensch, P., Cowan, T. & Hendon, H. H. An asymmetry in the IOD and ENSO teleconnection pathway and its impact on Australian climate. *J. Clim.* **25**, 6318–6329 (2012).
25. Chung, C. T. & Power, S. B. The non-linear impact of El Niño, La Niña and the Southern Oscillation on seasonal and regional Australian precipitation. *J. South. Hemisphere Earth Syst. Sci.* **67**, 25–45 (2017).
26. Dhame, S., Taschetto, A. S., Santoso, A. & Meissner, K. J. Indian Ocean warming modulates global atmospheric circulation trends. *Clim. Dyn.* **55**, 2053–2073 (2020).
27. Ihara, C., Kushnir, Y. & Cane, M. A. Warming trend of the Indian Ocean SST and Indian Ocean Dipole from 1880 to 2004. *J. Clim.* **21**, 2035–2046 (2008).
28. Cai, W. et al. Increased frequency of extreme Indian Ocean Dipole events due to greenhouse warming. *Nature* **510**, 254–258 (2014).
29. Hudson, D. et al. ACCESS-S1 The new Bureau of Meteorology multi-week to seasonal prediction system. *J. South. Hemisphere Earth Syst. Sci.* **67**, 132–159 (2017).
30. Zheng, B., Chapman, S. & Chenu, K. The value of tactical adaptation to El Niño–Southern Oscillation for East Australian wheat. *Climate* **6**, 77 (2018).
31. Keating, B. A. et al. An overview of APSIM, a model designed for farming systems simulation. *Eur. J. Agron.* **18**, 267–288 (2003).
32. Brown, H., Huth, N. & Holzworth, D. Crop model improvement in APSIM: using wheat as a case study. *Eur. J. Agron.* **100**, 141–150 (2018).
33. Innes, P. J., Tan, D. K. Y., Van Ogtrop, F. & Amthor, J. S. Effects of high-temperature episodes on wheat yields in New South Wales, Australia. *Agric. For. Meteorol.* **208**, 95–107 (2015).
34. Jeffrey, S. J., Carter, J. O., Moodie, K. B. & Beswick, A. R. Using spatial interpolation to construct a comprehensive archive of Australian climate data. *Environ. Model Softw.* **16**, 309–330 (2001).
35. Boer, M. M. et al. Future changes in climatic water balance determine potential for transformational shifts in Australian fire regimes. *Environ. Res. Lett.* **11**, 065002 (2016).
36. Williamson, G. J. et al. Measurement of inter-and intra-annual variability of landscape fire activity at a continental scale: the Australian case. *Environ. Res. Lett.* **11**, 035003 (2016).
37. Wang, B. et al. Australian wheat production expected to decrease by the late 21st century. *Glob. Chang. Biol.* **24**, 2403–2415 (2018).
38. Freeman, E. et al. ICOADS Release 3.0: a major update to the historical marine climate record. *Int. J. Climatol.* **37**, 2211–2232 (2017).
39. Thirumalai, K., DiNezio, P. N., Okumura, Y. & Deser, C. Extreme temperatures in Southeast Asia caused by El Niño and worsened by global warming. *Nat. Commun.* **8**, 1–8 (2017).
40. Titchner, H. A. & Rayner, N. A. The Met Office Hadley Centre sea ice and sea surface temperature data set, version 2: 1. Sea ice concentrations. *J. Geophys. Res. Atmos.* **119**, 2864–2889 (2014).

41. Deser, C., Alexander, M. A., Xie, S. P. & Phillips, A. S. Sea surface temperature variability: patterns and mechanisms. *Annu. Rev. Mar. Sci.* **2**, 115–143 (2010).
42. Heung, B., Bulmer, C. E. & Schmidt, M. G. Predictive soil parent material mapping at a regional-scale: a random forest approach. *Geoderma* **214**, 141–154 (2014).
43. Kuhn, M. Building predictive models in R using the caret package. *J. Stat. Softw.* **28**, 1–26 (2008).
44. Friedman, J. H. Greedy function approximation: a gradient boosting machine. *Ann. Stat.* **29**, 1189–1232 (2001).
45. Greenwell, B. M. pdp: an R package for constructing partial dependence plots. *R J.* **9**, 421 (2017).
46. Nicholls, N. Increased Australian wheat yield due to recent climate trends. *Nature* **387**, 484–485 (1997).
47. Archer, K. J. & Kimes, R. V. Empirical characterization of random forest variable importance measures. *Comput. Stat. Data Anal.* **52**, 2249–2260 (2008).

Acknowledgements

This work was part of a study investigating the impacts of and adaptation to our changing climate in Australia and China. This work is supported by the 2115 Talent Development Program of China Agricultural University (grant no. 1191-00109011), the Fundamental Research Funds for the Central Universities (grant no. 2022TC110), National Key R&D Program of China (grant no. 2020YFA0608004) and National Natural Science Foundation of China (grant no. 42088101).

Author contributions

B.W., P.F. and Q.Y. designed the research. P.F. and D.L.L. collected climate and soil data. P.F. ran machine learning and crop models. P.F. drew the figures. P.F. and B.W. wrote the draft manuscript. I.M., A.S.T., N.J.A., J.-J.L, A.D.K., Y.C., Y.L., D.L.L., Q.Y. and K.H. contributed to writing the manuscript.

Competing interests

The authors declare no competing interests.

Additional information

Supplementary information The online version contains supplementary material available at https://doi.org/10.1038/s43016-022-00613-9.

Correspondence and requests for materials should be addressed to Puyu Feng, Bin Wang or Kelin Hu.

Peer review information *Nature Food* thanks Weston Anderson and the other, anonymous, reviewer(s) for their contribution to the peer review of this work.